Journal of Histochemistry & Cytochemistry 2015, Vol. 63(5) 367–383

DOI: 10.1369/0022155415575027
jhc.sagepub.com
SAGE

Glial and Perivascular Structures in the Subfornical Organ: Distinguishing the Shell and Core

Károly Pócsai and Mihály Kálmán
Department of Anatomy, Histology and Embryology, Semmelweis University, Budapest, Hungary (KP, MK)

Summary
The subfornical organ (SFO) is a circumventricular organ with a chemosensitive function, and its vessels have no blood-brain barrier. Our study investigated the glial and vascular components in the SFO to determine whether their distributions indicate subdivisions, how to characterize the vessels and how to demarcate the SFO. To this end, we investigated glial markers (GFAP, glutamine synthetase, S100) and other markers, including vimentin and nestin (immature glia), laminin (basal lamina), β-dystroglycan (glio-vascular connections), and aquaporin 4 (glial water channels). We determined that the 'shell' of the SFO was marked by immunoreactivity for S100, GFAP and aquaporin 4. Nestin immunoreactivity was characteristic of the 'core'. Vimentin was almost evenly distributed. Glutamine synthetase immunoreactivity occurred in the shell but its expression was sparse. Vessels in the core were decorated with laminin but showed a discontinuous expression of aquaporin 4. Vimentin and GFAP staining was usually in separate glial elements, which may be related to their functional differences. Similar to other vessels in the brain, β-dystroglycan was detected along the shell vessels but laminin was not. The gradual disappearance of the laminin immunopositivity was attributed to the gradual disappearance of the perivascular space. Thus, our findings suggest that the shell and core glio-vascular structures are adapted to different sensory functions: osmoperception and the perception of circulating peptides, respectively.

Keywords
aquaporin 4, β-dystroglycan, circumventricular organs, nestin, tanycyte

Introduction

The subfornical organ (SFO) is one of the circumventricular organs in the brain, situated on the ventral surface of the fornix. For a general definition and description of the circumventricular organs, see, for example, McKinley et al. (2003), Vígh et al. (2004), and Sisó et al. (2010). Since the circumventricular organs have chemosensory and/or neurosecretory functions, they require free access to cerebral blood; i.e., they lack a blood-brain barrier (except for the subcommissural organ). Their vasculature is characterized by fenestrated capillaries and relatively large perivascular spaces into which dendrites and axons project (Dellmann 1998; Gross 1991; McKinley et al. 2003). The role of the SFO is well studied in terms of the perception of osmolarity, plasma sodium concentrations and angiotensin II levels, as well as with respect to signals for the central regulation of salt- and volume-homeostasis and blood pressure (for recent reviews see McKinley et al. 2003; Vígh et al. 2004). Receptors for further signaling polypeptides have also been found; for example, amylin, cholecystokinin, ghrelin, glucagon-like peptide-1, leptin and vasopressin (reviewed by McKinley et al. 2003).

The SFO is positioned below the ventral hippocampal commissure (Paxinos and Watson 1998) where the choroid

Received for publication March 16, 2014; accepted January 25, 2015.

Corresponding Author:
M. Kálmán, Department of Anatomy, Histology and Embryology, Semmelweis University, Tűzoltó 58, Budapest, H-1094, Hungary.
E-mail: kalman.mihaly@med.semmelweis-univ.hu

Table 1. Primary Antibodies Applied in the Study.

Marker	Antibody Species	Company	Catalogue Number	Dilution	Final Conc. (μg/mL)
Aquaporin 4	Rabbit**	Sigma-Aldrich (St Louis, MO)	a5371	1:200	1.5
β-dystroglycan	Mouse*	Novocastra (Newcastle-on-Tyne, UK)	ncl-b-dg	1:100	0.19
GFAP	Mouse*	Novocastra	ga5	1:100	100
GFAP	Rabbit**	DAKO (Glostrup, Denmark)	Z0334	1:500	2.8
Glutamine synthetase	Mouse*	Transduction Laboratories (Erembodegem, Belgium)	610518	1:100	2.5
Laminin 1	Rabbit**	Sigma-Aldrich	19393	1:100	5
Nestin	Mouse*	Millipore (Temecula, CA)	MAB-353	1:1000	1
RECA-1	Mouse*	Abcam (Cambridge, MA)	ab9774	1:1000	100
S100	Rabbit**	Sigma-Aldrich	s-2644	1:100	81
Vimentin	Mouse*	Calbiochem (Darmstadt, Germany)	IF01-100UG	1:1000	0.5
Vimentin	Chicken**	Novus Biologicals (Littleton, CO)	NB300-223	1:1000	20

GFAP, glial fibrillary acidic protein; Conc., concentration. *Monoclonal antibody; **polyclonal antibody.

plexuses of the lateral and third ventricles converge. The choroid epithelium here continues into the SFO ependyma (Dempsey 1968). Its postero-dorsal surface is a pial surface (Gross 1991; Spoerri 1963), whereas the ventral surface is ventricular, and its anterodorsal surface contacts the ventral hippocampal commissure. Thus, the SFO faces three compartments: the cerebral tissue, the ventricle and the subarachnoid space. From the main part of the SFO, the ventral and dorsal protrusions extend, like 'stalks' of the organ (Akert et al. 1961). The main artery of the SFO is the subfornical branch of the anterior cerebral artery, which reaches the SFO from a caudal direction. For a detailed description of the vascular architecture of the SFO see Spoerri (1963).

Revising the former, rather complicated subdivision systems of the SFO, McKinley et al. (2003) considered it sufficient to distinguish a 'core' and a 'shell'. The shell is continuous with the ventral and dorsal stalks, and it is rich in neurons providing the majority of the efferent fibers of the SFO, whereas axons from the core course mainly to the bed nucleus of the stria terminalis. Calbindin-immunoreactive neurons have been found exclusively in the core, whereas calretinin-immunoreactive neurons are confined to the shell (McKinley et al. 2003).

The present study investigates the glial and vascular components of the SFO according to the following questions: i) How does their distribution indicate subdivisions; e.g., shell versus core? ii) How are the vessels of the SFO distinguished from the 'common' cerebral vessels? and iii) How can one demarcate the SFO from the adjacent cerebral tissue and from the ventricular and subarachnoid spaces?

To this end, we investigated various substances (see also Table 1). Laminin is a ubiquitous, major component of the basal laminae (for its role in brain vessels, see e.g. Hallmann et al. 2005). Laminin immunopositivity, however, is not detected in the vessels in the mature brain, except in the Virchow-Robin spaces and in vessels of the circumventricular organs (Krum et al. 1991). Dystroglycan, on the other hand, plays an important role in glio-vascular coupling (Tian et al. 1996; Wolburg et al. 2009). It consists of an α- and a β-subunit. The α-dystroglycan subunit is an extracellular protein that binds to laminin and other components of the basal lamina. The β-dystroglycan subunit is a transmembrane protein that anchors the α-dystroglycan to the membrane of the glial (or other) cells. Its immunoreactivity delineates the brain vessels but not the extracerebral ones (Szabó and Kálmán 2008; Uchino et al., 1996; Zaccaria et al., 2001).The other end of the β-dystroglycan subunit forms a complex with dystrophin, dystrobrevin and other proteins. The complex integrates aquaporin 4 water-channels, ion-channels and signaling systems. Aquaporin 4 is the major form of aquaporins in the brain (Venero et al. 2001). It plays a crucial role in cell volume homeostasis.

Astroglia produce basal lamina in the central nervous system (Liesi et al. 1983; Jucker et al. 1996), their vascular end-feet contain the dystroglycan complex (Tian et al. 1996; Wolburg et al. 2009) and they induce the formation of the blood-brain barrier (Janzer and Raff 1987; Abbott 2002). The widely accepted immunohistochemical marker for astroglia is glial fibrillary acidic protein (GFAP) (Bignami et al. 1980), an intermediate filament protein. However, according to several studies, not all astrocytes can be detected using GFAP. It is useful, therefore, to examine other astroglial markers, such as glutamine synthetase and S100 protein (Ludwin et al. 1976; Martinez-Hernandez et al. 1977). We also investigated staining for vimentin and nestin, proteins that occur in immature glia (Dahl et al. 1981; Hockfield and McKay 1985; Zerlin et al. 1995). Nestin may be particularly relevant, as it has recently been

Table 2. Secondary Antibodies Applied in the Study.

Conjugated	Antibody Species	Type	Absorbed light / Emitted light (nm)	Company	Catalogue Number	Dilution	Final Conc. (μg/mL)
Alexa Fluor 488	Rabbit	Donkey	488/519	Invitrogen (Carlsbad, CA)	A21206	1:500	4
Alexa Fluor 555	Mouse	Donkey	555/565	Invitrogen	A31570	1:500	4
Alexa Fluor 488	Chicken	Goat	488/519	Invitrogen	A11039	1:500	4

Conc., concentration.

reported to play a role in adult neurogenesis in the circumventricular organs (Bennett et al. 2009; Sanin et al. 2013; Wei et al. 2002).

Materials & Methods

Animals

Fourteen adult rats (Wistar) of either sex weighing 250 to 300 g were used. The animals were supplied with food (rat chow from Charles River Laboratories; Wilmington, MA) and water ad libitum, and kept on a 12/12 hr light-dark cycle. All experimental procedures were performed in accordance with the guidelines of European Communities Council Directive (86/609/EEC).

Fixation and Sectioning

The animals were deeply anesthetized with ketamine and xylazine (20 and 80 mg/kg, respectively, i.m.) and perfused through the aorta with 100 ml 0.9% sodium chloride followed by 300 ml 4% paraformaldehyde in 0.1 M phosphate buffer (pH 7.4). After perfusion, brains were removed and post-fixed in the same fixative for one day at 4°C. Tissue blocks containing the SFO were embedded into agarose, and serial sections (thickness, 50 μm; 5–6 sections per animal) were cut by a vibration microtome (Leica VT 1000S; Leica Microsystems, Wetzlar, Germany) in the coronal (11 animals), horizontal (2 animals) or sagittal (3 animals) planes.

Immunohistochemistry

Immunohistochemistry was performed as previously described (Bagyura et al. 2010; Pócsai et al. 2010). Briefly, floating sections were pretreated with 20% normal goat serum diluted in phosphate-buffered saline (PBS; Sigma-Aldrich, St. Louis, MO) for 90 min to block the non-specific binding of antibodies. This and the following steps were followed by an intensive wash and stirring in PBS (30 min, at room temperature). Primary immunoreagents were diluted as shown in Table 1 in PBS containing 0.5% Triton X-100 and 0.01% sodium azide. Sections were incubated for 40 hr at 4°C. Fluorescent secondary antibodies (Table 2) were used at room temperature for 3 hr. The sections were finally washed in PBS (1 hr, room temperature), mounted onto microscope slides, cover-slipped in a mixture of glycerol and double distilled water (1:1) and sealed with lacquer. Control sections were treated identically, except for the omission of the primary antibody. No structure-bound fluorescence labeling was observed in these specimens.

Double-Labeling Immunofluorescence Reactions

Antigens were detected simultaneously using primary antibodies of different species (see Table 1) applied in parallel in the same incubation medium. The protocol was as described above.

Endothelial Marker, RECA-1

The presence and position of the vessels were identified using the endothelial marker RECA-1 (Duijvestijn et al. 1992; Maolood and Meister 2009). In some experiments, RECA-1 immunolabeling was combined with other immunostaining, either simultaneously or subsequently (in a separate immunohistochemical reaction on the same specimen), and these cases are indicated in the Figure legends.

Confocal Laser Scanning Microscopy and Digital Imaging

Slides were photographed by a Radiance-2100 confocal laser scanning microscope (Bio-Rad; Hercules, CA). Green and red colors on the photomicrographs correspond to the emitted colors of the fluorescent dyes, as shown in Table 2. Digital images were processed using Photoshop 9.2 software (Adobe Systems; Mountain View, CA) with minimal adjustments for brightness and contrast.

Results

Laminin–β-dystroglycan Double Immunolabeling

In sagittal sections, the three surfaces of the SFO were recognized: the pial, the ventricular and the ‘cerebral’ or ‘parenchymal’ (fused to the ventral hippocampal commissure) surfaces (Fig. 1A). Two thin extensions of the SFO (stalks) were observed extending dorsally and ventrally

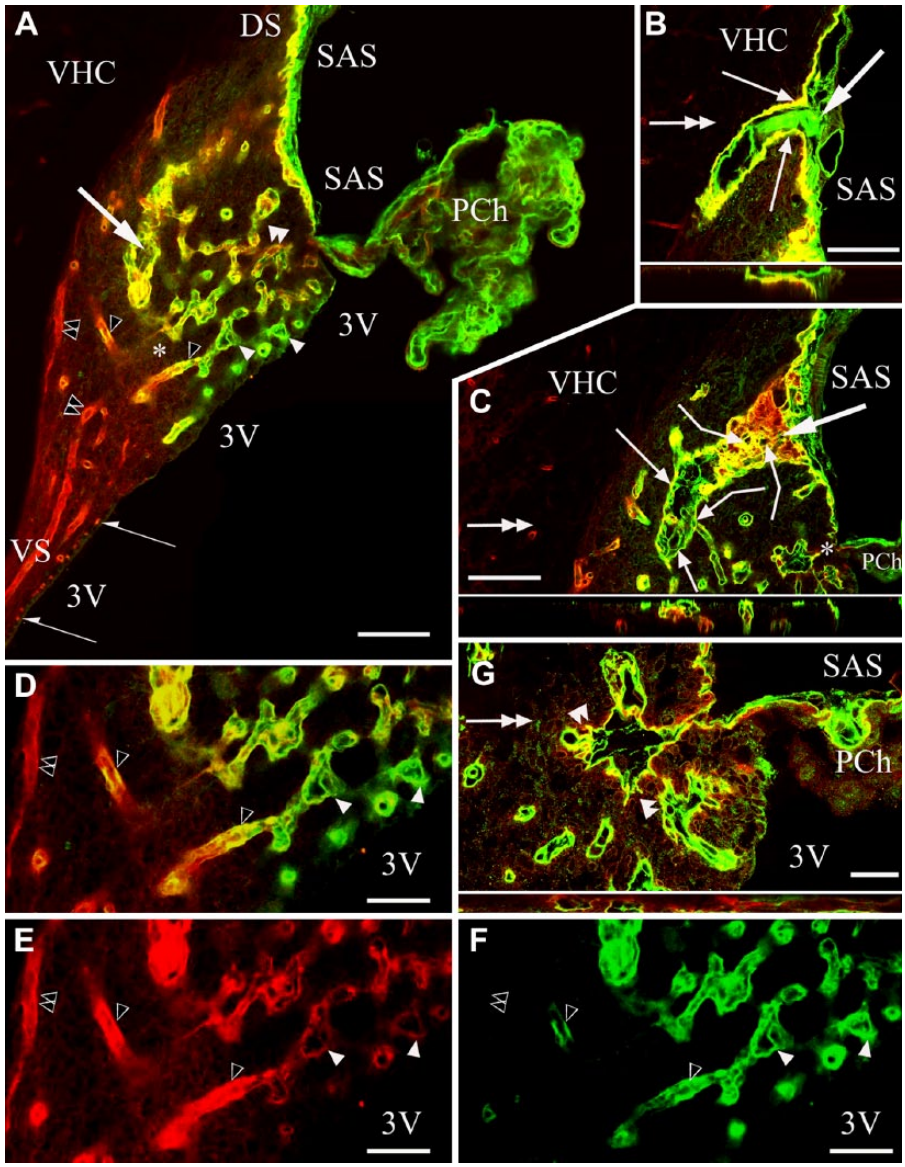

Figure 1. Laminin and β-dystroglycan immunoreactivity in sagittal sections of the subfornical organ (SFO). In subsequent section planes near the mid-sagittal plane, laminin is green, β-dystroglycan, red and co-localization, yellow. Empty arrowheads, 'single-walled' vessels, immunoreactive for laminin and β-dystroglycan. Double empty arrowheads, 'single-walled' vessels, immunoreactive only for β-dystroglycan. (A) Three surfaces of the SFO. Cerebral ('parenchymal') extends to the ventral hippocampal commissure (VHC); pial, to the subarachnoid space (SAS); ependymal (not immunoreactive), to the third ventricle (3V). The pial and ependymal surfaces are separated by the attachment of the choroid plexus (PCh). DS, VS: dorsal and ventral 'stalks', respectively. (B) A large vessel surrounded by an in-folding of the pial surface. Inset: Z-stack of (B) in the plane indicated by the double-headed arrow. (C) An oblique section of the large vessel seen in (B). Broken arrows: connections with small vessels. Inset: Z-stack of (C) in the plane indicated by the double-headed arrow. Large arrows in Panels (A–C) point to the same large vessel in different focus planes. (D) Detail of (A) around the asterisk. Open arrowheads point to the same structures as in (A). (E, F) The monochromatic components of (D). (G) Detail of (C) around the asterisk, enlarged. small vessels in an in-folding of the pial surface. Inset: Z-stack of (G) in the plane indicated by the double-headed arrow. Arrows indicate in-foldings of the pial surface around large vessels. Note the perivascular space. Double arrowheads indicate 'double-walled' vessels, with two laminin-immunopositive layers. The outer layer shows β-dystroglycan immunoreactivity (green plus red or yellow). Arrowheads also indicate 'double-walled' vessels, with two laminin-immunopositive layers, the outer layer shows a weak β-dystroglycan immunoreactivity [yellowish color, note the identical vessels in (D and E)]. Scale (A–C) 100 μm (also for the insets); (D–F) 50 μm; (G) 25 μm (also for the inset).

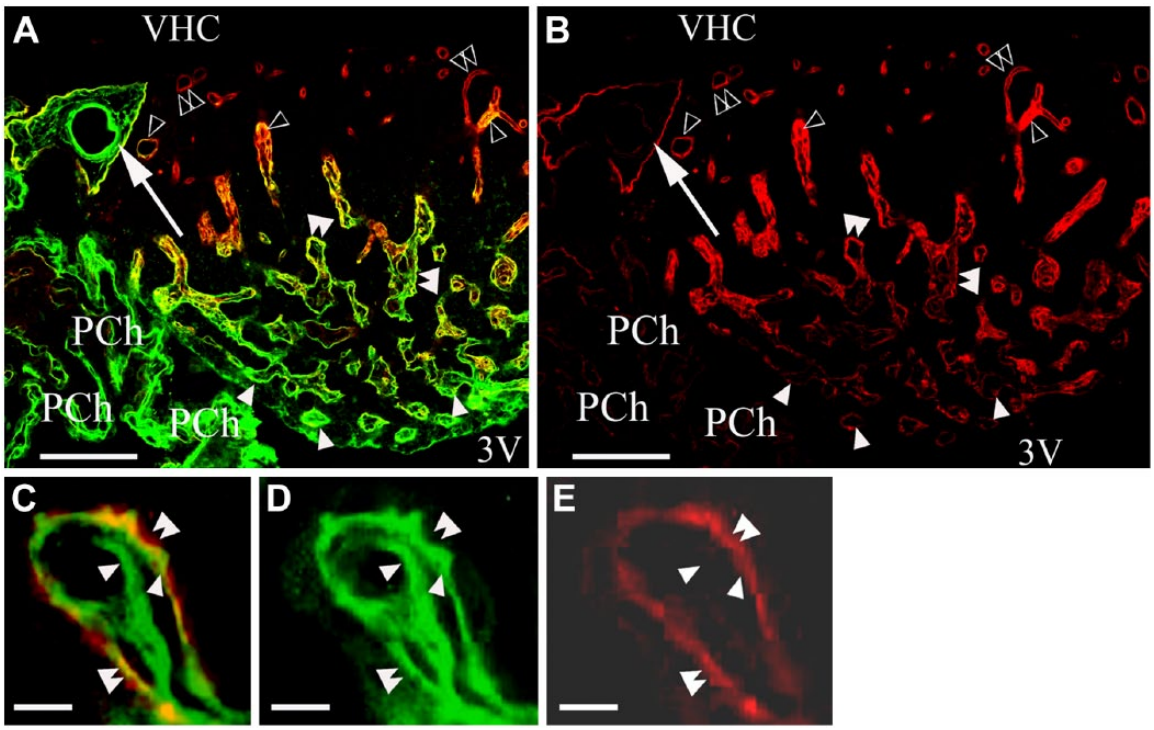

Figure 2. Laminin and β-dystroglycan double immunostaining in a horizontal section of the subfornical organ (SFO). Laminin is stained green, β-dystroglycan, red, and co-localization of the two, yellow. (A) Horizontal section shows alterations in the perivascular immunoreactivity for laminin and β-dystroglycan from the ventricular surface to the 'cerebral' surface. Large arrows point to large vessels in pial in-foldings on the lateral side of the SFO. Other marks are the same as that described for Figure 1. (B) The monochromatic red component of (A). Marks in (B) are identical to those in (A). (C) Cross-section of a 'double-walled'vessel, two laminin-immunopositive layers (arrowheads) with β-dystroglycan immunoreactivity in the outer layer (green plus red, or yellow; double arrowheads). (D, E) Monochromatic components of (C). Marks in (C–E) are identical. Scale (A and B) 100 μm; (C–E) 10 μm. Abbreviations: VHC, ventral hippocampal commissure; SAS, subarachnoid space; 3V, third ventricle.

(Fig. 1A). At the border between the ependymal and pial surfaces, the choroid epithelial lamina was attached to the SFO. The pial surface was lined with laminin and β-dystroglycan-immunoreactive layers (Fig. 1A–1C). This surface formed in-foldings into the substance of the SFO (Fig. 1A–1C) from where laminin-immunoreactive vessels entered the SFO. Around these vessels, perivascular spaces were found as continuations of the subarachnoid space (Fig. 1B and 1G). In small vessels, the perivascular spaces were narrow and therefore the vessels seemed to be 'double-walled' (Fig. 1D–1I). In the deeper vessels, perivascular spaces were not visible and their 'wall' was a single layer.

Four types of vessels were distinguished (Figs. 1, 2):

Type (a)'double-walled': two laminin-immunopositive layers enclosing a perivascular space, but only the corresponding monochromatic photo showed a weak β-dystroglycan immunoreactivity along the outer 'wall';
Type (b) 'double-walled': two laminin-immunopositive layers similar to Type a) but the outer 'wall' showed immunoreactivity for β-dystroglycan;
Type (c) 'single-walled': immunoreactive for laminin and β-dystroglycan, but no detectable perivascular space;
Type (d) 'single-walled': immunoreactive only for β-dystroglycan, as for other vessels throughout the brain.

From the central area of the SFO heading toward its periphery, the vessels gradually changed from Type (a) to Type (d), although the intermediate Type (c) was relatively less frequently observed. The 'stalks' had only Type (d) vessels. Horizontal sections (Fig. 2A, 2B) better demonstrated the distribution of the different vessel types and revealed large 'holes' not only in the middle (see Fig. 1) but also in the lateral part of the SFO. The immunostaining of their 'walls' (laminin plus β-dystroglycan) indicated that they were in-foldings of the pial surface (see also Fig. 1) and surrounded large vessels. We used an endothelial marker RECA-1 (Fig. 3A–3I) to confirm that the laminin- and/or β-dystroglycan-immunoreactive 'walls' really surrounded vessels. RECA-1 immunopositivity was found within both laminin-immunopositive layers (Fig. 3D–3I), whereas the β-dystroglycan immunoreactivity was found outside of them (Fig. 3C and 3F–3I).

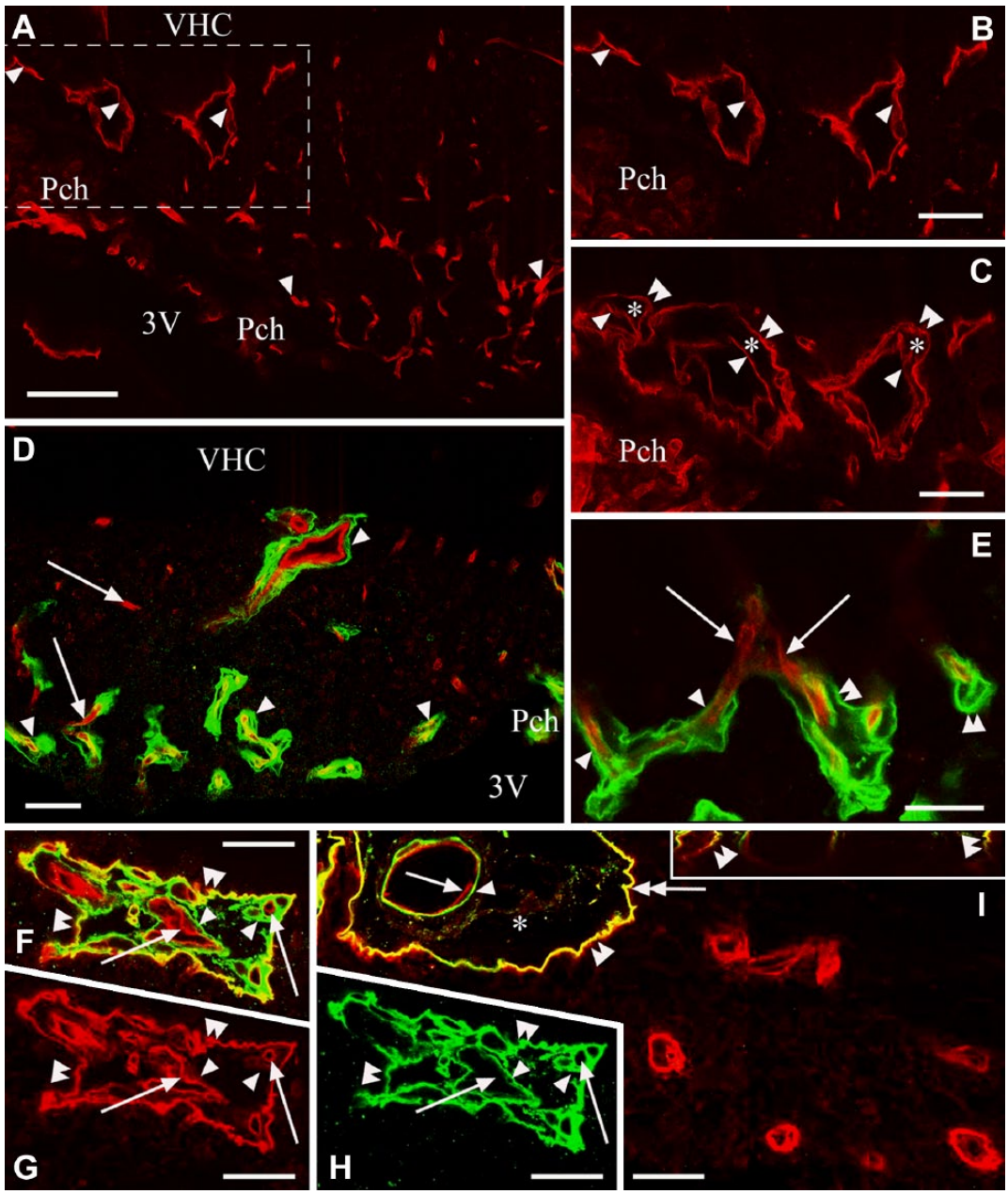

Figure 3. Combination of laminin and/or β-dystroglycan immunostaining with immunostaining for the endothelial marker RECA-1. (A) RECA-1 immunostaining of the subfornical organ (SFO). Horizontal section. Arrowheads indicate vessels. (B and C) The dashed box area in (A). In (C) the section has been additionally immunostained for β-dystroglycan. An outer 'wall' (double arrowheads) and perivascular space (asterisk) are now visible around the endothelium (arrowheads) of the vessels. (D and E) Laminin (green) and RECA-1 (red) double immunolabeling in a frontal section. Arrowheads indicate a laminin-immunopositive layer detectable around the endothelium. Arrows show that no laminin-immunopositive layer is detectable around the endothelium. Double arrowheads show a double laminin-immunopositive layer. (F) Immunostaining against laminin (green), RECA-1 (red) and β-dystroglycan (red). Double arrowheads mark an in-folding of the pial surface (a common outer 'wall') that is immunopositive for laminin and β-dystroglycan in close localization (yellow), as shown in Figures 1 and 2. Arrowheads mark laminin-immunopositive layers around vessels (inner 'walls'). Arrows indicate RECA-1-immunopositive endothelium within the inner wall. (G and H) The monochromatic components of (F). Marks in (F–H) are in identical positions. (I) A large vessel with the same immunostaining as applied in (F). Double arrowhead indicates the laminin–β-dystroglycan double-immunoreactive (yellow) outer 'wall'; single arrowhead indicates the laminin-immunoreactive inner 'wall'. Arrow shows endothelial RECA-1 immunoreactivity. Asterisk indicates the perivascular space. Inset: Z-stack in the plane indicated by a double-headed arrow shows the laminin–β-dystroglycan double-immunoreactive (yellow) outer 'wall'. Scale (A) 100 μm; (B–D) 50 μm; (E–I) 25 μm (also for the inset). Abbreviations: 3V, third ventricle; PCh, choroid plexus; VHC, ventral hippocampal commissure.

Immunostaining against GFAP, Vimentin, and Co-localization with β-Dystroglycan and Laminin

GFAP immunoreactivity marked the peripheral shell of the SFO, which included the large lateral vessels (Fig. 4A) and also the dorsal and ventral stalks. In the rest of the SFO (termed the core), GFAP-immunoreactive processes were seen only around vessels and the large middle 'hole' (Fig. 4A and 4D). Vimentin immunoreactivity was quite evenly distributed in the SFO (Fig. 4B, 4C), usually in long glial processes (Fig. 4B and 4E). The ependyma was also intensely immunoreactive for vimentin (Fig. 4B): the cells were cuboidal laterally (shell) but flat in the center (core, Fig. 4B; see also Fig. 5A, 5B). When we combined β-dystroglycan immunolabeling, which delineated the vessels, with either vimentin or GFAP immunostaining (Fig. 4C and 4D, respectively), it was clear that every vessel had a glial cover.

Both the laminin-immunopositive and -immunonegative vessels have perivascular glia, which was determined using immunostaining against RECA-1 (Fig. 4G, 4H). The structures of the perivascular glia were, however, variable. The immunolabeled perivascular glial sheaths were continuous in the shell but not in the core (see, for example, Fig. 4F). The co-localization of vimentin and GFAP was relatively infrequent. Long vimentin- or GFAP-immunoreactive or double-labeled glial processes extended into both the ventral stalk (Fig. 5A) and the dorsal stalk (not shown). The perivascular glial sheaths were continuous in the shell (Fig. 5B, 5C) but, in the core, they seemed to be loose and discontinuous, even when both glial markers were together, and were either formed by club-like processes (Figs. 4F, 5D) or by an onion-like organization of processes (Fig. 5E–5H).

Cell bodies giving rise to perivascular glial processes were only occasionally observed. GFAP-immunoreactive processes originated from parenchymal cell bodies (Fig. 5B and 5F), whereas some of the vimentin-immunoreactive processes originated from ependymal cells (Figs. 4E, 4F, 5B). The proportion of the vimentin- and/or GFAP-immunoreactive perivascular glial processes was variable. Even where GFAP predominated, there were processes that were immunoreactive only for vimentin and vice versa (Fig. 5E, 5F) but GFAP and vimentin were only infrequently co-localized in the same process. The presence of vessels within the glial sheath was confirmed by immunostaining against RECA-1 (Fig. 5C, 5G, 5H).

Other Components: Glutamine Synthetase, S100, Nestin and Aquaporin4

The glutamine synthetase-immunoreactive cells had short, thick processes. They were seen mainly around the large lateral vessels but too scarcely to delineate a territory (Fig. 6A). S100-immunoreactive cells marked the shell (Fig. 6B, 6C), similar to the GFAP immunoreactivity (Fig. 4A). The core was almost completely S100-immunonegative (Fig. 6C). Some glutamine synthetase or S100-immunoreactive cell bodies had GFAP-immunoreactive processes (Fig. 6D–6F and 6G–6I, respectively). Both S100 and vimentin immunoreactivities were found in the ependymal cells but, in the cell bodies, S100 predominated, whereas in the processes, vimentin did (Fig. 6J–6L). The nestin-immunoreactive processes formed groups around the vessels in the core (Fig. 7A) but they were almost absent in a shell-like area (Fig. 7A). Nestin and vimentin double immunolabeling (Fig. 7B) revealed that the nestin-immunoreactive glial processes were also vimentin-immunoreactive. The pial surface was free of nestin-immunoreactive processes. A densely packed aquaporin 4 immunoreactivity marked a shell (Fig. 8A, 8B), similar to the immunoreactivity of GFAP or S100 (Fig. 4A and 6B, respectively), but aquaporin 4 was confined to the vessels in the core. Along the vessels, aquaporin 4 was continuous in the shell but discontinuous in the core (Fig. 8A–8C). Staining was intense in the cuboidal ependyma of the shell (Fig. 8A–8C), but the flat ependyma of the core was almost totally immunonegative (Fig. 8A–8C). Aquaporin 4 immunoreactivity was also seen along the pial surface (Fig. 8A, 8B). Comparing the distribution of the immunoreactivity of aquaporin 4 to that of vimentin, co-localization was scarce (Fig. 8D–8G). For GFAP and aquaporin 4 double immunolabeling, the co-localization was complete around the vessels in the shell, whereas it was only partial around the vessels of the core (Fig. 8H).

Discussion

Glial Immunostaining Patterns Can Separate 'Shell' and 'Core'

Immunoreactivity for S100, GFAP and aquaporin 4, but not vimentin, clearly define the shell and core regions in the SFO. GFAP (Kálmán and Hajós 1989; Goren et al. 2006) and aquaporin 4 (Venero et al. 2001; Goren et al. 2006) have previously been detected in the SFO, but the shell–core distribution has not been described. In our previous study, *Wisteria floribunda* lectin binding also marked a shell-like territory (Pócsai and Kálmán 2014). It is notable that the landscape of the SFO depends highly on the section level; indeed, the most rostral and most caudal frontal sections may reflect the shell structure without a considerable portion of the core. This estimate of the distribution of the shell and core can be seen in the sketches in Figure 9, which summarizes the results.

Glutamine synthetase-immunoreactive cells were too scarce to delineate the shell. However, Berger and Hediger (2000) found that the immunoreactivity of the glutamate transporter GLT-1 delineated a shell in the SFO, whereas, for another glutamate transporter, GLAST, immunoreactivity was found throughout the organ. The scarce occurrence

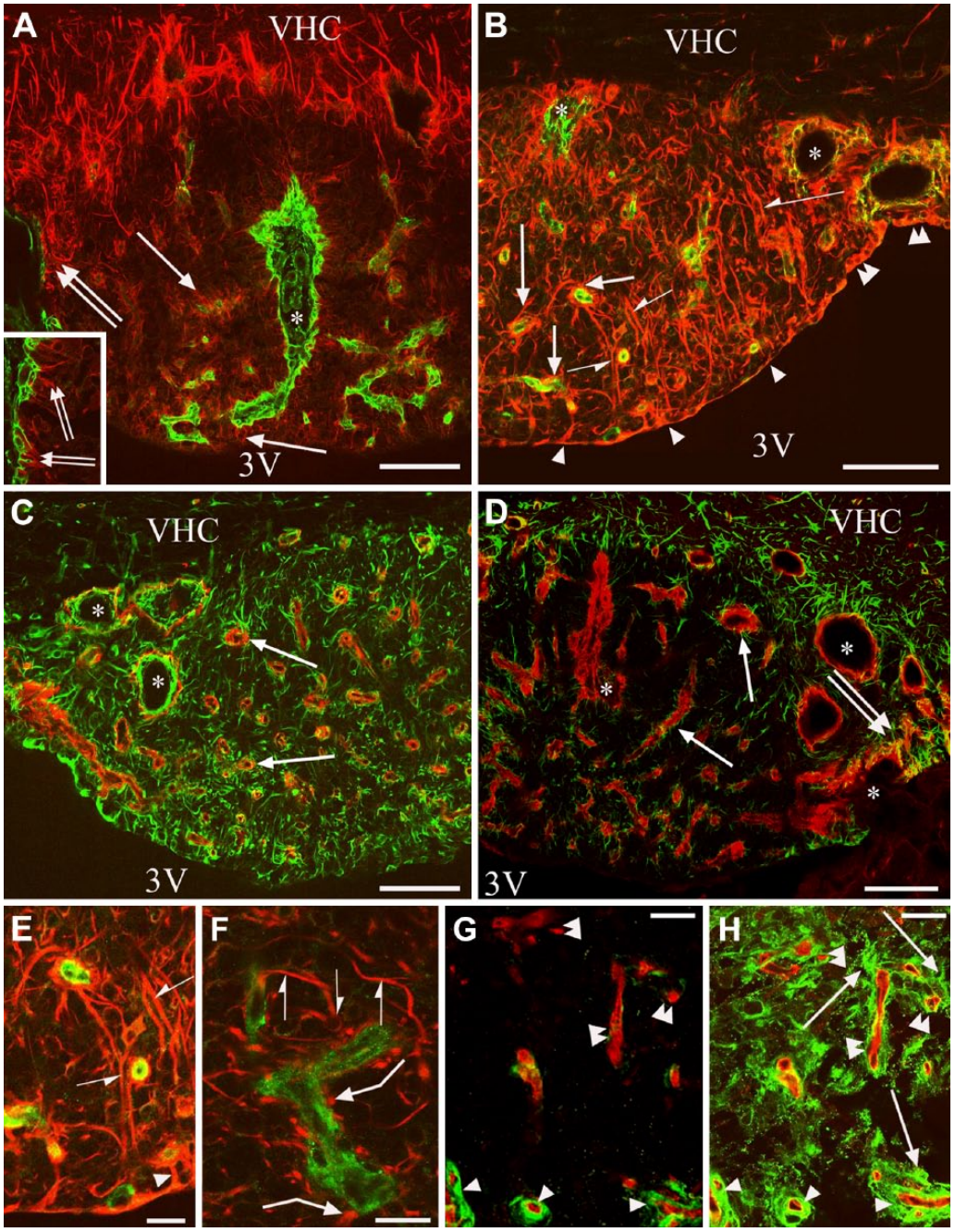

Figure 4. β-dystroglycan or laminin immunostaining combined with immunostaining against GFAP or vimentin. Double labeling is performed on frontal sections. Asterisks indicate vessel-containing in-foldings of the pial surface surrounded by glial processes. (A) GFAP (red) and laminin (green) double immunolabeling. GFAP immunoreactivity marks a 'shell' that is free from laminin-immunopositive vessels. Arrows indicate glial processes around the laminin-immunolabeled vessels in the 'core'. Double arrows mark glial processes extending to the pial surface. Inset: enlarged detail of the pial in-folding near the asterisk. (B) Vimentin (red) and laminin (green) double immunolabeling. Arrowheads point to flat ependyma covering the central part of the subfornical organ (SFO). Double arrowheads mark cuboidal ependyma covering the lateral part of the SFO. Arrows are as in (A). Half arrows mark non-ependymal long processes. (C) Vimentin (green) and β-dystroglycan (red) double immunolabeling. Arrows show that every β-dystroglycan-immunolabeled vessel is surrounded by glial processes. (D) GFAP (green) and β-dystroglycan (red) double immunolabeling. Arrows are as in (C); double arrows mark glial processes extending to the pial surface. (E and F) Vimentin-immunoreactive (red) glial processes around laminin-immunoreactive (green) vessels. (E) is an enlargement of (B). Half arrows mark the continuous perivascular glia, non-ependymal long processes. Arrowhead shows continuous perivascular glia, ependymal process. Bent arrows show discontinous perivascular glia with club-like endings. (G) RECA-1 (red) and laminin (green) double immunolabeling. Arrowheads show laminin-immunoreactive vessels. Double arrowheads show vessels with minimal or no laminin immunoreactivity. (H) Subsequent immunostaining for GFAP (green) on the vessels seen in (G). Arrows show GFAP-immunoreactive glial processes; other marks are as in (G). Scale (A–D) 100 μm (inset, 50 μm); (E–H) 25 μm. Abbreviations: 3V, third ventricle; VCH, ventral hippocampal commissure.

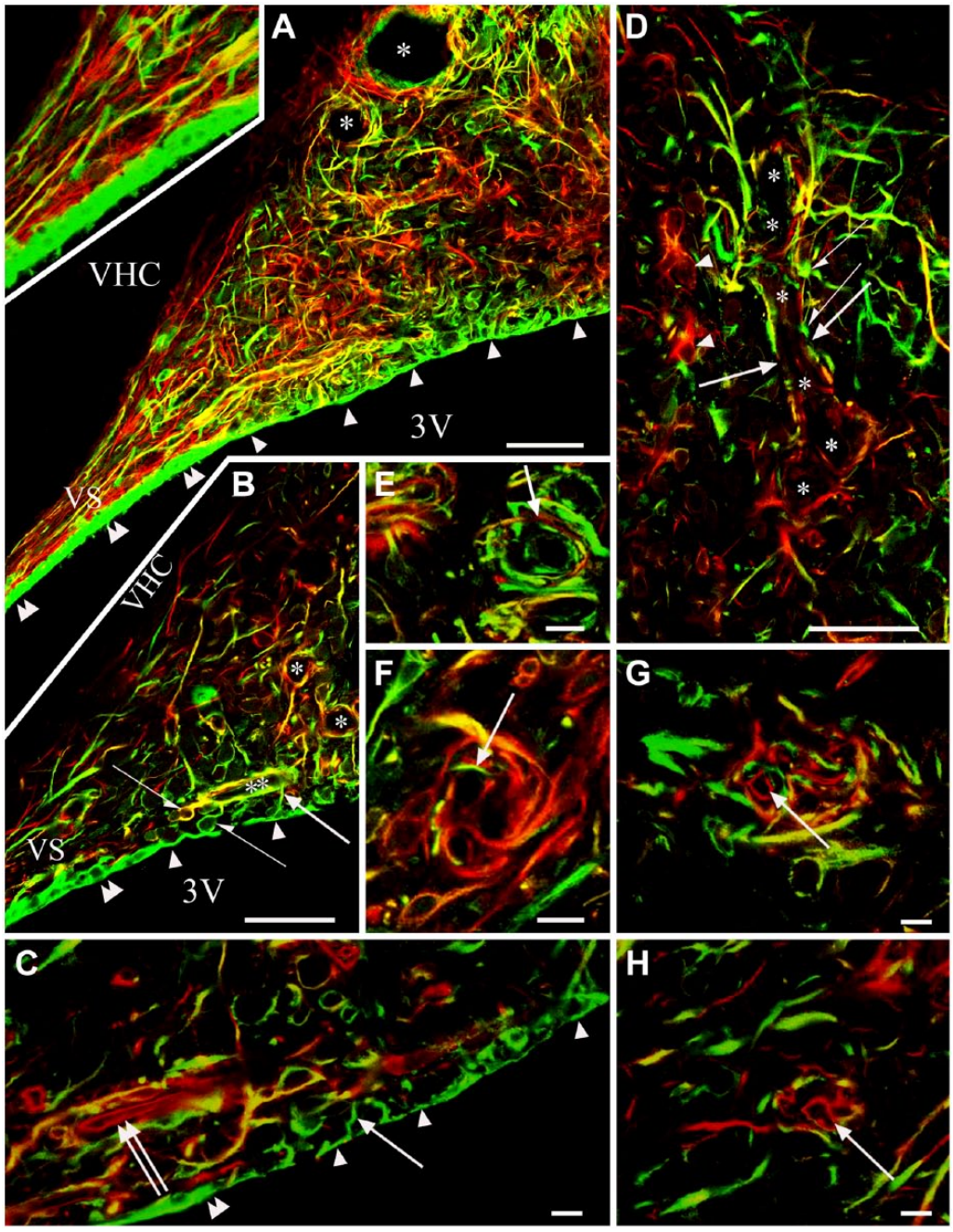

Figure 5. Vimentin (green) and GFAP (red) double immunolabeling. Note the relatively infrequent co-localizations. (A, B) Sagittal section. (A) The lower part of the subfornical organ (SFO) with the ventral 'stalk'. Arrowheads show flat ependyma covering the 'core' of the SFO. Double arrowheads mark cuboidal ependyma. Asterisks indicate glial elements of various immunostaining around a vessel-like space. Inset: Enlarged detail of (A). The ventral stalk (VS) contains long parallel glia processes. (B) The lower part of the SFO with the ventral 'stalk'. Half arrows show the non-ependymal round glial cell with processes to the same vessel. Arrows mark the ependymal processes to a near vessel. Other marks are as in (A). (C) Perivascular glia counterstained with anti-RECA-1 to label the endothelium (red, double arrow) within the glial sheath. Other marks are as in (B). (D) Glial elements of various immunostaining around a space (asterisks), probably a vessel. Half arrows mark club-like perivascular glial endings; arrows show immunonegative segments; arrowheads show astrocytes. (E–H) Onion-like arrangements of perivascular processes. Arrows show a GFAP-immunoreactive process among vimentin-immunoreactive ones (E), a vimentin-immunoreactive process among GFAP-immunoreactive ones (F), endothelium followed a counterstaining against RECA-1 (G, H). Scale (A, B and D) 50 μm (inset, 35 μm); (C and E–H) 10 μm. Abbreviations: 3V, third ventricle; VHC, ventral hippocampal commissure; VS, ventral stalk.

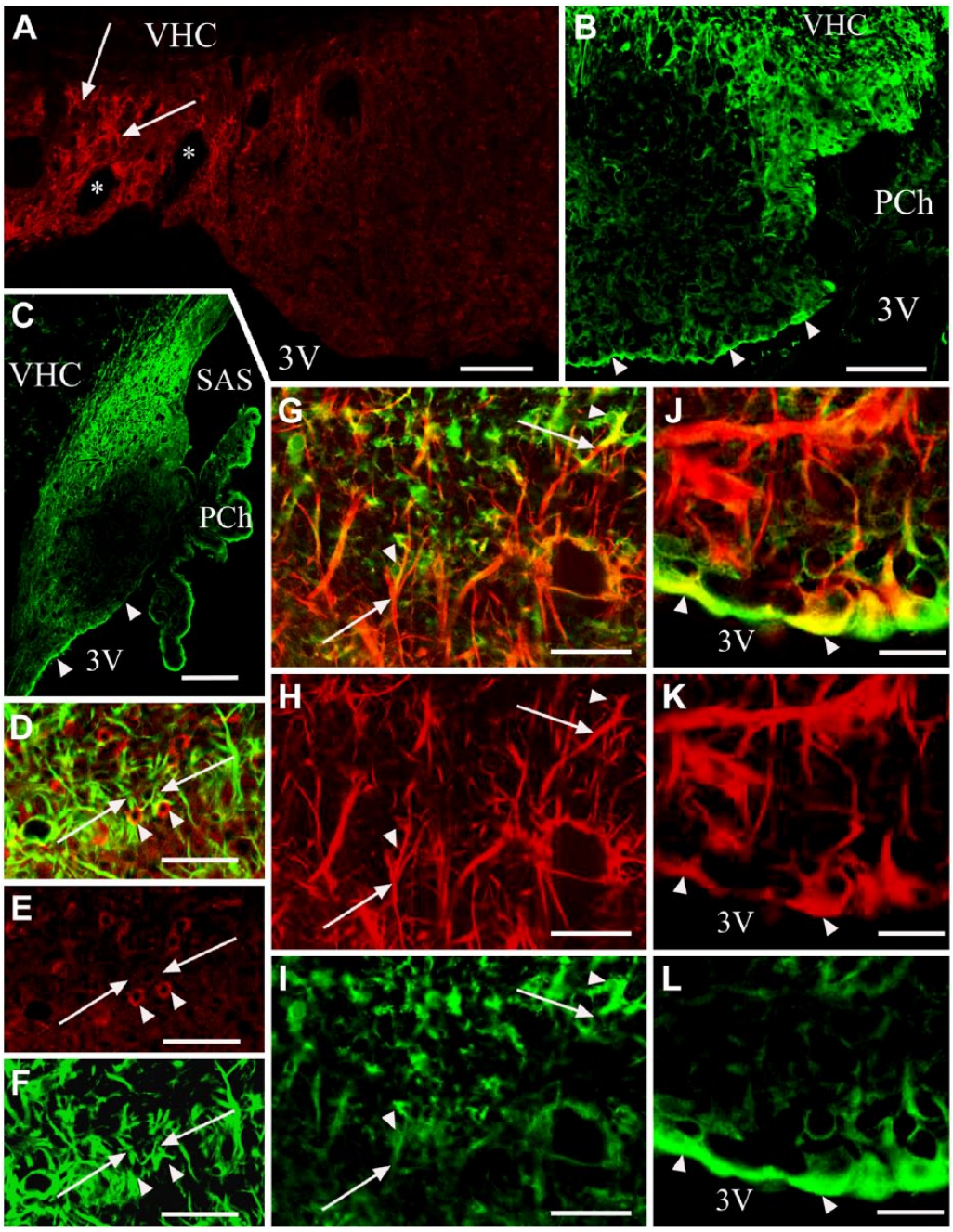

Figure 6. Glutamine synthetase and S100 immunoreactivities. (A) Glutamine synthetase immunolabeling in a frontal section. Arrows mark glutamine synthetase-immunoreactive cells around the large lateral vessels (asterisks). (B and C) S100 immunolabeling of frontal and sagittal sections, respectively. S100 immunoreactivity marks the shell. Arrowheads indicate S100-immunoreactive ependyma. (D) Glutamine synthetase (red) and GFAP (green) double immunolabeling. Arrowheads indicate glutamine synthetase-immunoreactive cells with GFAP-immunoreactive processes (arrows). (E and F) Monochromatic components of (D); marks in (D–F) are identical. (G) S100 (green) and GFAP (red) double immunolabeling. Arrowheads show S100-immunoreactive cells with GFAP-immunoreactive processes (arrows). (H and I) Monochromatic components of (G); marks in (G–I) are identical. (J) S100 (green) and vimentin (red) double immunolabeling. S100 predominates in the ependymal cell bodies, whereas vimentin predominates in the processes. Arrowheads indicate co-localization (yellow). (K and L) Monochromatic components of (J); marks in (J–L) are identical. Abbreviations: 3V, third ventricle; PCh, choroid plexus; SAS, subarachnoid space; VCH, ventral hippocampal commissure. Scale (A–C) 100 μm; (D–I) 50 μm; (J–L) 25 μm.

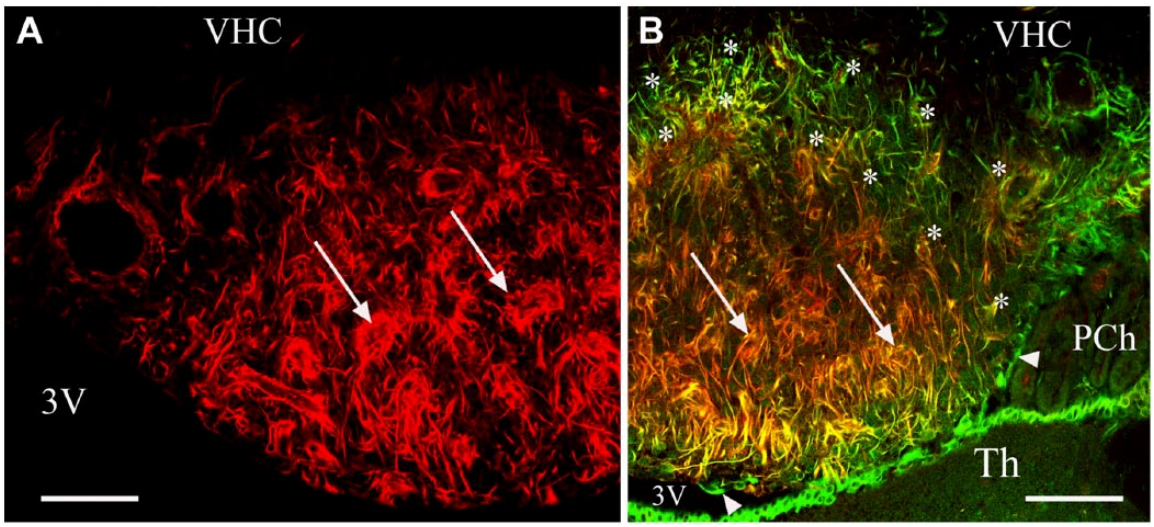

Figure 7. Distribution of the immunopositivity of nestin. (A) Nestin immunolabeling in a frontal section. Asterisks mark the shell, where nestin immunoreactivity is almost absent. Arrows indicate nestin-immunoreactive processes around vessel-like spaces. (B) Nestin (red) and vimentin (green) double immunolabeling in a frontal section. Arrows are as in (A); note, here, the co-localization (yellow or reddish-yellow). Asterisks indicate a shell-like area with immunoreactivity for vimentin but not nestin. Arrowheads show that ependymal cells lack nestin-immunoreactivity. The thalamus is also covered by ependyma. Scale, 100 µm. Abbreviations: 3V, third ventricle; Th, thalamus; PCh, choroid plexus; VHC, ventral hippocampal commissure.

of glutamine synthetase is surprising, but similar observations have been published for the area postrema (D'Amelio et al. 1987) and the median eminence (Okere and Waterhouse 2004).

Glial processes in the core were selectively labeled for nestin, which co-localized with vimentin. Nestin has been shown to form co-polymers with vimentin (Eliasson et al. 1999; Marvin et al. 1998; Menet et al. 2001). Bennett et al. (2009) found that neurospheres can develop in vitro from nestin-containing SFO cells (also immunopositive for GFAP and vimentin), and that S100-immunopositive cells took up bromdeoxyuridine, indicating neurogenesis. The long processes we observed may have a guidance function, like radial glia, in this case.

New Elements of the Glial Architecture

Usually, tanycytes and astrocytes are mentioned as characteristic glial elements of the SFO (Langlet et al. 2013). Our results modify this with two details: (i) the SFO contains numerous 'unipolar' (i.e. with one process), non-ependymal cells displaying GFAP or vimentin immunoreactivity and (ii) the long glial processes found in the core originate mainly from S100-immunoreactive cell bodies of the shell; i.e., they were not tanycytic processes. The long glial processes of the dorsal and ventral stalks of the SFO are supposed to be parallel with the afferent and efferent axons interconnecting the SFO with septal and hypothalamic nuclei (Akert et al. 1961; McKinley et al. 2003).

Surfaces: Ventricular, Pial and Cerebral

The 'cerebral surface' of the SFO was only recognizable by the quite sharp border of the shell toward the ventral hippocampal commissure. The pial surface was similar to that found throughout the brain (see, for example, Szabó and Kálmán 2008): its laminin-immunoreactive layer represents the basal lamina toward the pial tissue, whereas the β-dystroglycan immunopositivity is attributed to the attaching subpial glial end-feet.

Aquaporin 4 has also been found along the pial surface of the brain (Jung et al. 1994; Nielsen et al. 1997). The ventricular surface of the SFO was covered with ependymocytes and tanycytes (see, for example, Dellmann 1998; Sisó et al. 2010), which had processes terminating on nearby vessels. On the periphery of the SFO, over the shell, the ependyma was similar to that found generally in the brain ventricles: it was cuboidal and immunoreactive to vimentin and S100 (Schnitzer et al. 1981; Didier et al. 1986) and aquaporin 4 (Jung et al. 1994; Nielsen et al. 1997).The core ependyma, however, was different: it was flat and almost devoid of aquaporin 4 immunoreactivity, and may correspond to the 'squamous' ependyma described in the 'central' part of the SFO (Gross 1991).

Significance of the Vascular Immunoreactivity for Laminin and β-Dystroglycan

Where vessels enter the brain, their 'wall' is reduced to an endothelial tube with a basal lamina. Another basal lamina,

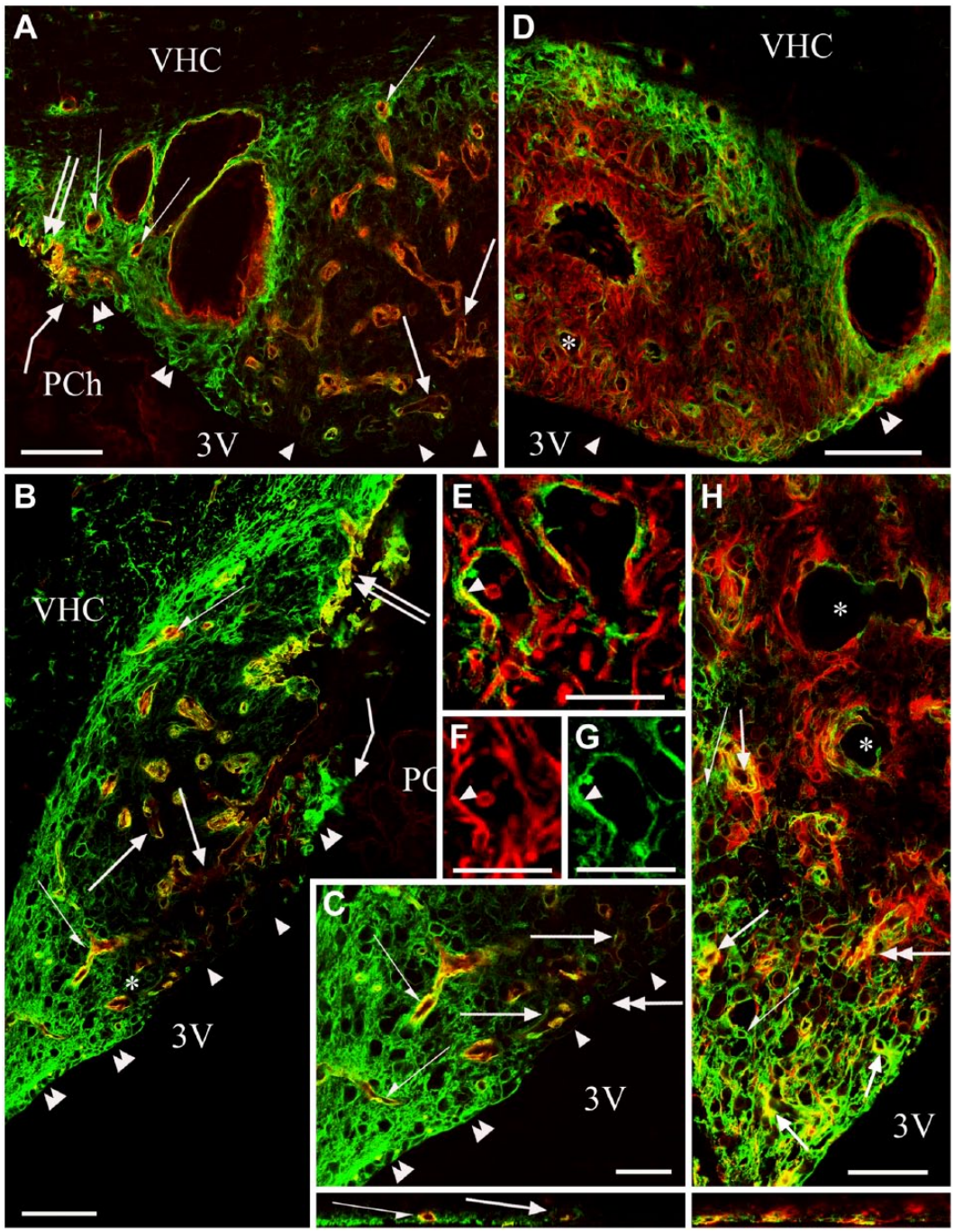

Figure 8. Distribution of the immunopositivity of aquaporin 4. (A and B) Aquaporin 4 (green) and β-dystroglycan (red) double immunolabeling in frontal and sagittal sections, respectively. Aquaporin 4 immunoreactivity labels a shell. Arrows and half arrows show β-dystroglycan-immunopositive vessels with discontinuous or continuous aquaporin 4 immunoreactivity in the core and in the shell, resp. Double arrows show the pial surface; bent arrows show the attachment of the (missing) choroid epithelium. Double arrowheads and arrowheads indicate that the ependyma is cuboidal and aquaporin 4 immunopositive over the shell but not over the core, respectively. (C) Enlargement of (B) around the asterisk; marks are as in (A and B). Inset: Z-stack in the plane indicated by the double-headed arrow. (D, E) Aquaporin 4 (green) and vimentin (red) double immunolabeling in a frontal section. (D) Double arrowheads and arrowheads are as in (B). Asterisk marks the area enlarged in (E). Aquaporin 4 immunoreactivity labels the shell but co-localization with vimentin is rather infrequent (arrow in E). (F and G) Monochromatic components of (E); marks in (E–G) are identical. (H) Aquaporin 4 (green) and GFAP (red) double immunolabeling in a sagittal section (lower part of the SFO). Arrows mark aquaporin 4–GFAP co-localization (yellow). Half arrows indicate cells bearing solely aquaporin 4 immunoreactive processes. Asterisks mark vessels of the core that show discontinuous aquaporin 4 immunostaining. Inset: Z-stack of (H) in the plane indicated by the double-headed arrow. Scale, (A, B and D) 100 μm; (C and H) 50 μm (also for the insets); (E–G) 25 μm. Abbreviations: 3V, third ventricle; PCh, choroid plexus; VHC, ventral hippocampal commissure.

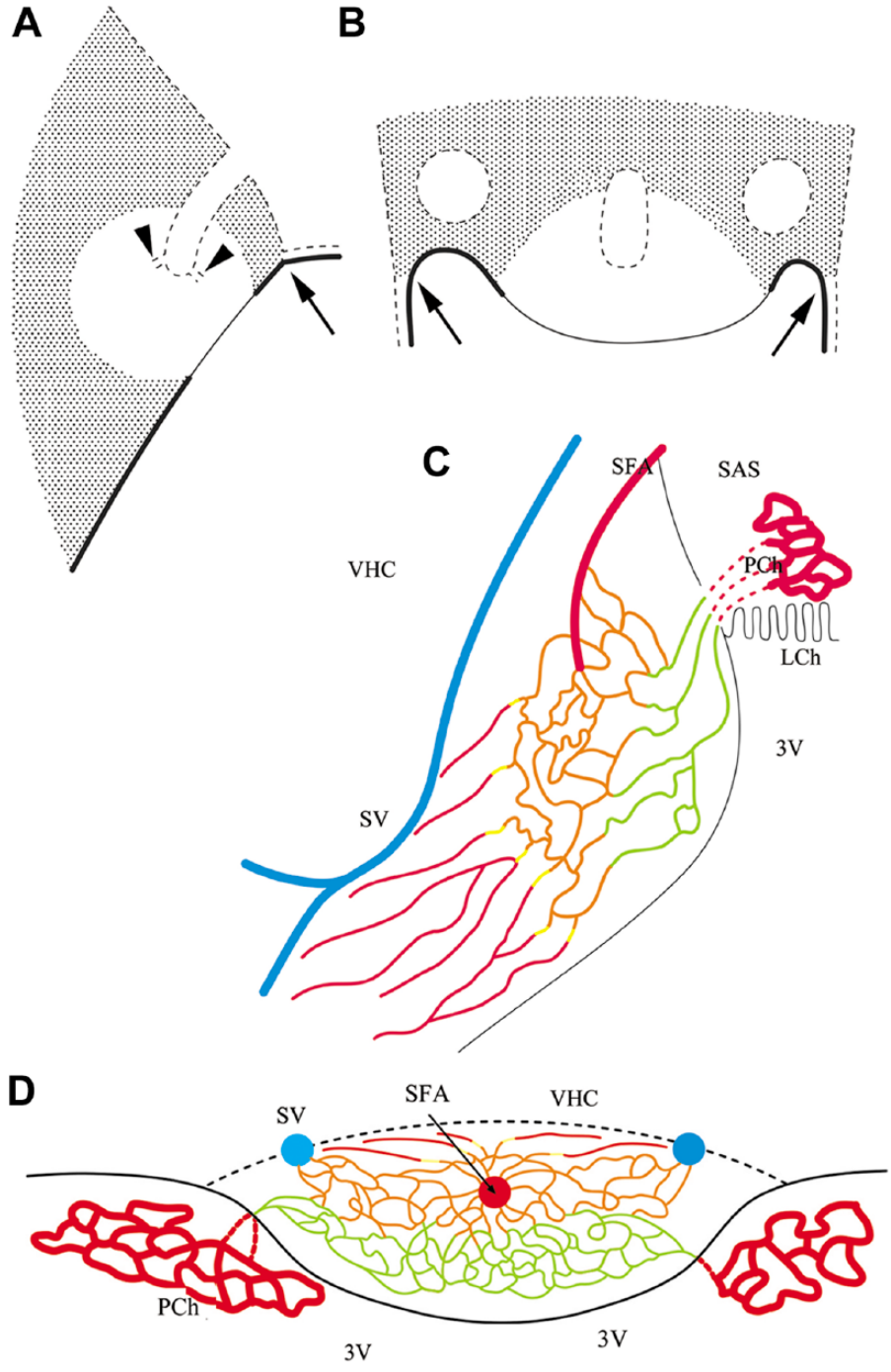

Figure 9. Sketches summarizing the results. (A and B) Representations of the shell and the core of the SFO in mid-sagittal and horizontal sections, respectively. Shadowed area shows the shell, which is marked by immunopositivity for GFAP, S100 and aquaporin 4; the vessels are immunopositive for β-dystroglycan but not laminin [type (d)], and have continuous glial sheaths also immunopositive for aquaporin 4. The clear area marks the core, which is rich in nestin but not in GFAP immunopositivity. The vessels are immunoreactive for both β-dystroglycan and laminin [types (a), (b) and (c)], whereas the immunoreactivity to GFAP, vimentin and aquaporin 4 is not continuous around them. Note that the shell/core proportion depends on the section plane, and some sections may represent only the shell. Continuous line marks the ependymal (ventricular) surface, which is immunopositive for vimentin and S100; the thick line symbolizes cuboidal cells, which are immunopositive also for aquaporin 4; the thin line symbolizes flat cells without aquaporin 4 immunopositivity; and the dotted line indicates the pial surface with glial end-feet, which is immunopositive for laminin, β-dystroglycan and aquaporin 4. Arrows mark the site of attachment of the choroid plexus. Holes delineated by dotted lines mark the sections of the in-foldings of the pial surface, which contain the large vessels of the organ (see C and D). Arrowheads mark the small tube trunks symbolize the emerging, vessel-containing channels; the vessels are not shown. (C and D) The vascular system. Sketches in sagittal and horizontal sections, respectively, are based on the sketches of Spoerri (1963) but labeling the differences of the vessels. Abbreviations: 3V, third ventricle; LCh, choroid lamina; PCh, choroid plexus; SAS, subarachnoid space; SFA, subfornical artery; SV, septal vein; VHC, ventral hippocampal commissure. Color code (refers only to the thin lines): vessels of Type (a): green; Type (b): orange; Type (c) yellow, Type (d) red. Note, the septal vein and the subfornical artery are not in the same plane, but we followed the sketch of Spörri (1963) in this matter.

which is produced by astroglia, covers the pial surface of the brain and lines the Virchow-Robin spaces. At the end of the Virchow-Robin spaces, the two basal laminae fuse together (Caley and Maxwell 1970; Bär and Wolff 1972; Marin-Padilla 1985; Sixt et al. 2001; Hallmann et al. 2005). According to Krum et al. (1991), the lack of the cerebrovascular laminin-immunoreactivity is due to a masking effect of the fusion of the two basal laminae, which 'hides' the laminin epitopes and makes them inaccessible for antibodies. Laminin immunopositivity, therefore, may indicate vessel segments where the two laminae are not completely fused, as the cleft between them is not recognizable under light microscopy. For more detailed discussions, see Krum et al. (1991) and Szabó and Kálmán (2004). The β-dystroglycan immunopositivity, which delineates the cerebral vessels (Szabó and Kálmán 2008; Uchino et al., 1996; Zaccaria et al., 2001), is attributed to perivascular glial end-feet (Tian et al. 1996; Walburg et al. 2009).

Double-walled Vessels: Vessels in Tunnels of the Pial Surface

The 'holes' in the SFO sections are actually Virchow-Robin spaces. The relatively large vessels in the middle and lateral holes may correspond to the subfornical artery and to the septal veins, respectively, on the basis of the figures of Spoerri (1963). The outer 'walls' of the vessels are actually tunnel-like invaginations of the pial surface. The β-dystroglycan-immunoreactive layer is formed by the perivascular glial end-feet (Tian et al. 1996; Walburg et al. 2009) on the outer side of the laminin-immunoreactive basal lamina of the brain tissue. The inner 'wall' is the vascular basal lamina, which is immunoreactive only for laminin. The perivascular spaces are supposed to be continuous with the subarachnoid space.

Laminin-β-dystroglycan Double Labeling Differentiates Vessel Types

Applying the same lettering as in the Results:

- Types (a) and (b) are 'double walled' vessels, with wide perivascular spaces and separate parenchymal and vascular basal laminae. The weak β-dystroglycan immunostaining refers to weak glio-vascular connections in Type (a).
- Type (c) are 'single walled' vessels in which laminin is still detectable and co-localized with β-dystroglycan. It indicates that the basal laminae are not fused completely but their space is very narrow; i.e., invisible at the light microscopy level. It is a transitory type between Types (b) and (d).
- Type (d) are 'single walled' vessels, in which the lack of laminin immunopositivity indicates that the basal laminae are fused completely, as seen throughout the brain.

Our vessel classification may correspond to the types distinguished in the SFO by electron microscopy (Gross 1991), which indicated a gradual alteration from the middle of the SFO (Type III with a considerable perivascular space) through the transitional Type I toward the periphery (Type II, without perivascular space as seen throughout the brain). We found a similar transition, from Type (a) and (b) in the core via Type (c) to Type (d) in the shell.

Vimentin and GFAP in Different Perivascular Glial End-feet

Whereas in the shell the perivascular glial sheath was continuous, in the core, it seemed to be discontinuous and loose. Vimentin and GFAP frequently occurred separately in different glial elements intermingled with each other, even when they surrounded the same vessels. Otherwise, where vimentin occurs in the astrocytes of the mature brain (corpus callosum, Bergmann-glia, reactive glia; see Schnitzer et al. 1981; Janeczko 1993), it is co-localized with GFAP. Different intermediate filament compositions indicate different features and functions of the end-feet (Galou et al. 1994; Menet et al. 2001). Pixley and de Vellis (1984) suggested, for example, that vimentin-containing glial processes are especially capable of transport from fluid compartments.

Glio-vascular Structures and the Lack of the Blood-Brain Barrier

The loose perivascular glial sheath, the weak β-dystroglycan immunostaining [Type (a) vessels], and the discontinuous immunoreactivity of aquaporin 4, which characterized the core vessels, may be indirect signs of weak glio-vascular connections and leaky vessels. Nico et al. (2001, 2003) found that aquaporin 4 is a marker of the maturation and integrity of the blood-brain barrier. Shell vessels [Type (d)] were delineated with a continuous aquaporin 4 immunopositivity, as seen throughout the brain (Goren et al. 2006; Nielsen et al. 1997).

Where there is a perivascular space, the glial end-feet have actually no vascular contacts. Bouchaud et al. (1989) as well as Gross (1991) suggested that the larger the glia-endothelium distance, the weaker the astroglial ability to induce the formation of the blood-brain barrier in the endothelium. A 'leakage' through the endothelium and the perivascular space mutually support each other. Experiments with silver granules leaving the vessels where the blood-brain barrier is missing (Dempsey 1968) proved the innermost part of the SFO as a privileged area of leakage. Gross (1991) also found that the blood-brain (or brain-blood) transport was more intense in the central part of the SFO.

The core proved to be more sensitive to the angiotensin II level, which may be attributed to an ease in blood-brain barrier traversal here (McKinley et al. 2003), and this may apply to other macromolecules as well.

Aquaporin 4: Correlation with GFAP and osmometric function

The outstanding occurrence of aquaporin 4 in the shell corresponds to the distribution of GFAP (see also Venero et al. 2001; Goren et al. 2006) but seems to be independent from that of β-dystroglycan, to which otherwise the aquaporin 4 is anchored in the astroglial end-feet (Amiry-Moghaddam et al. 2004). It is in accordance with the electron microscopic description of Nielsen et al. (1997) that aquaporin 4 in the SFO was not confined to the astroglial end-feet but it was distributed in the whole cells. The cytoskeleton may affect the channel proteins (Yoneda et al. 2001; Nico et al. 2004). No aquaporin 4 co-localization with vimentin was seen, except for in the ependyma.

Aquaporin 4 is thought to increase the osmosensitivity, since it facilitates water diffusion. The water moves easily towards high osmolarity, which results in a cell deformation that may be the trigger for osmoreceptors (Noda 2007; Noda and Sakuta 2013; Venero et al. 2001; Wells 1998). A type of sodium channel involved in the detection of this ion has been described in the glial cells of the SFO (Noda 2007), and is known to be activated by endothelin-3 (Noda and Sakuta 2013). Endothelin distribution also forms a shell in its co-localization with GFAP (Gebke et al. 2000). Hence, the different glio-vascular structures in the core and shell may serve different detection functions (peptides versus small molecules and osmoperception).

Evolutionary Correlation to the Choroid Plexus?

The structure of the SFO represents a kind of transition between the choroid plexus and the brain. This is even suggested by its position at the attachment of the choroid plexus (Akert et al. 1961). Continuity between the choroid plexus and the SFO vessels has also been suggested (Spoerri 1963). The system of deep perivascular spaces decreases the distance between the subarachnoid and ventricular compartments. In the plexus, which is also regarded a kind of circumventricular organ (see Vígh et al. 2004), the tissue between the two compartments is reduced to the choroid epithelium. Dempsey (1968) noted that the development of the area postrema and SFO (which he termed "intercolumnar tubercle") shares features with the development of the choroid plexus. Like the SFO, the area postrema is also positioned at the attachment of the choroid plexuses. This raises the possibility that the SFO (and maybe the area postrema, too) were the forerunners of the choroid plexus.

In conclusion, the shell and core components are distinguished by the immunoreactivity of their glia. The shell vessels resemble other cerebral vessels, whereas the features of the core vessels seem to correlate with the lack of a blood-brain barrier. The gradual disappearance of laminin immunoreactivity may be attributed to the gradual narrowing and disappearance of the perivascular space. The perivascular vimentin and GFAP expression occur mainly in separate glial elements, indicating functional differences. Long glial processes also originate from non-ependymal cells, in addition to ependymal tanycytes. The ependyma covering the core lacks aquaporin 4. The shell and core glio-vascular structures seem to be adapted to different sensory functions: osmoperception and the perception of circulating peptides, respectively.

Acknowledgments

The authors are thankful to Dr. Sándor Nardai and Dr. Árpád Dobolyi for the generous gift of the anti RECA-1 antibody. The technical assistance of Andrea Őz, Erzsébet Horváthné Oszwald and Szilvia Deák is highly appreciated. We would like to thank Dr. Mark Eyre for English proof-reading.

Declaration of Conflicting Interests

The authors declared no potential conflicts of interest with respect to the research, authorship, and/or publication of this article.

Funding

The authors disclosed receipt of the following financial support for the research, authorship, and/or publication of this article: The study was supported by the PhD School of Semmelweis University.

References

Abbott NJ (2002). Astrocyte-endothelial interactions and blood-brain barrier permeability. J Anat 200:629-638.

Adorján I, Kálmán M (2009). Distribution of beta-dystroglycan immunopositive globules in the subventricular zone of rat brain. Glia 57:657-666.

Akert K, Potter HD, Andreson JW (1961). The subfornical organ in mammals. I. Comparative and topographical anatomy. J Comp Neurol 116:1-13.

Amiry-Moghaddam M, Frydenlund DS, Ottersen OP (2004). Anchoring of aquaporin 4 in brain: molecular mechanisms and implications for the physiology and pathophysiology of water transport. Neuroscience 129:999-1010.

Bagyura Z, Pócsai K, Kálmán M (2010). Distribution of components of basal lamina and dystrophin-dystroglycan complex in the rat pineal gland: differences from the brain tissue and between the subdivisions of the gland. Histol Histopathol 25:1-14.

Bär T, Wolff JR (1972). The formation of capillary basement membranes during internal vascularization of the rat's cerebral cortex. Z Zellforsch Mikrosk Anat 133:231-248.

Bennett L, Yang M, Enikolopov G, Iacovitti L (2009). Circumventricular organs: a novel site of neural stem cells in the adult brain. Mol Cell Neurosci 41:337-347.

Berger UV, Hediger MA (2000). Distribution of the glutamate transporters GLAST and GLT-1 in rat circumventricular organs, meninges, and dorsal root ganglia. J Comp Neurol 421:385-399.

Bignami A, Dahl D, Seiler MW (1980). Neurofilaments in the chick embryo during early development. I. Immunofluorescent study with antisera for neurofilament protein. Dev Neurosci 3:151-161.

Bouchaud C, Le Bert M, Dupouey P (1989). Are close contacts between astrocytes and endothelial cells a prerequisite condition of a blood-brain barrier? The rat subfornical organ as an example. Biol Cell 67:159-165.

Caley DW, Maxwell DS (1970). Development of the blood vessels and extracellular spaces during postnatal maturation of rat cerebral cortex. J Comp Neurol 138:31-47.

D'Amelio FE, Mehler WR, Gibbs MA, Eng LF, Wu JY (1987). Immunocytochemical localization of glutamic acid decarboxylase (GAD) and glutamine synthetase (GS) in the area postrema of the cat. Light and electron microscopy. Brain Res 410:232-244.

Dahl D, Rueger DC, Bignami A, Weber K, Osborn M (1981). Vimentin, the 57 000 molecular weight protein of fibroblast filaments, is the major cytoskeletal component in immature glia. Eur J Cell Biol 24:191-196.

Dellmann HD (1998). Structure of the subfornical organ: a review. Microsc Res Tech 41:85-97.

Dempsey EW (1968). Fine-structure of the rat's intercolumnar tubercle and its adjacent ependyma and choroid plexus, with especial reference to the appearance of its sinusoidal vessels in experimental argyria. Exp Neurol 22:568-589.

Didier M, Harandi M, Aguera M, Bancel B, Tardy M, Fages C, Calas A, Stagaard M, Møllgård K, Belin MF (1986). Differential immunocytochemical staining for glial fibrillary acidic (GFA) protein, S-100 protein and glutamine synthetase in the rat subcommissural organ, nonspecialized ventricular ependyma and adjacent neuropil. Cell Tissue Res 245:343-351.

Duijvestijn AM, van Goor H, Klatter F, Majoor GD, van Bussel E, van Breda Vriesman PJ (1992). Antibodies defining rat endothelial cells: RECA-1, a pan-endothelial cell-specific monoclonal antibody. Laboratory Investigation. 66:459-466.

Eliasson C, Sahlgren C, Berthold CH, Stakeberg J, Celis JE, Betsholtz C, Eriksson JE, Pekny M (1999). Intermediate filament protein partnership in astrocytes. J Biol Chem 274:23996-24006.

Galou M, Pournin S, Ensergueix D, Ridet JL, Tchelingerian JL, Lossouran L, Privat A, Babinet C, Dupouey P (1994). Normal and pathological expression of GFAP promoter elements in transgenic mice. Glia 12:281-293.

Gebke E, Müller AR, Pehl U, Gerstberger R (2000). Astrocytes in sensory circumventricular organs of the rat brain express functional binding sites for endothelin. Neuroscience 97:371-381.

Goren O, Adorján I, Kálmán M (2006). Heterogeneous occurrence of aquaporin 4 in the ependyma and in the circumventricular organs in rat and chicken. Anat Embryol (Berl) 211:155-172.

Gross PM (1991). Morphology and physiology of capillary systems in subregions of the subfornical organ and area postrema. Can J Physiol Pharmacol 69:1010-1025.

Hallmann R, Horn N, Selg M, Wendler O, Pausch F, Sorokin LM (2005). Expression and function of laminins in the embryonic and mature vasculature. Physiol Rev 85:979-1000.

Hockfield S, McKay RD (1985). Identification of major cell classes in the developing mammalian nervous system. J Neurosci 5:3310-3328.

Janeczko K (1993). Co-expression of GFAP and vimentin in astrocytes proliferating in response to injury in the mouse cerebral hemisphere. A combined autoradiographic and double immunocytochemical study. Int J Dev Neurosci 11:139-147.

Janzer RC, Raff MC (1987). Astrocytes induce blood-brain barrier properties in endothelial cells. Nature 325:253-257.

Jucker M, Tian M, Ingram DK (1996). Laminins in the adult and aged brain. Mol Chem Neuropathol 28:209-218.

Jung JS, Bhat RV, Preston GM, Guggino WB, Baraban JM, Agre P (1994). Molecular characterization of an aquaporin cDNA from brain: candidate osmoreceptor and regulator of water balance. Proc Natl Acad Sci U S A 91:13052-13056.

Kálmán M, Hajós F (1989). Distribution of glial fibrillary acidic protein (GFAP)-immunoreactive astrocytes in the rat brain. I. Forebrain. Exp Brain Res 78:147-163.

Krum JM, More NS, Rosenstein JM (1991). Brain angiogenesis: variations in vascular basement membrane glycoprotein immunoreactivity. Exp Neurol 111:152-165.

Langlet F, Mullier A, Bouret SG, Prevot V, Dehouck B (2013). Tanycyte-like cells form a blood-cerebrospinal fluid barrier in the circumventricular organs of the mouse brain. J Comp Neurol 521:3389-3405.

Liesi P, Dahl D, Vaheri A (1983). Laminin is produced by early rat astrocytes in primary culture. J Cell Biol 96:920-924.

Ludwin SK, Kosek JC, Eng LF (1976). The topographical distribution of S-100 and GFA proteins in the adult rat brain: an immunohistochemical study using horseradish peroxidase-labelled antibodies. J Comp Neurol 165:197-207.

Maolood N, Meister B (2009). Protein components of the blood-brain barrier (BBB) in the brainstem area postrema-nucleus tractus solitarius region. J Chem Neuroanat 37:182-195.

Marin-Padilla M (1985). Early vascularization of the embryonic cerebral cortex: Golgi and electron microscopic studies. J Comp Neurol 241:237-249.

Martinez-Hernandez A, Bell KP, Norenberg MD (1977). Glutamine synthetase: glial localization in brain. Science 195:1356-1358.

Marvin MJ, Dahlstrand J, Lendahl U, McKay RD (1998). A rod end deletion in the intermediate filament protein nestin alters its subcellular localization in neuroepithelial cells of transgenic mice. J Cell Sci 111 (Pt 14):1951-1961.

McKinley MJ, McAllen RM, Davern P, Giles ME, Penschow J, Sunn N, Uschakov A, Oldfield BJ (2003). The sensory circumventricular organs of the mammalian brain. Adv Anat Embryol Cell Biol 172:III-XII, 1-122, back cover.

Menet V, Giménez y Ribotta M, Chauvet N, Drian MJ, Lannoy J, Colucci-Guyon E, Privat A (2001). Inactivation of the glial fibrillary acidic protein gene, but not that of vimentin, improves neuronal survival and neurite growth by modifying adhesion molecule expression. J Neurosci 21:6147-6158.

Nico B, Frigeri A, Nicchia GP, Quondamatteo F, Herken R, Errede M, Ribatti D, Svelto M, Roncali L (2001). Role of

aquaporin-4 water channel in the development and integrity of the blood-brain barrier. J Cell Sci 114:1297-1307.

Nico B, Frigeri A, Nicchia GP, Corsi P, Ribatti D, Quondamatteo F, Herken R, Girolamo F, Marzullo A, Svelto M, Roncali L (2003). Severe alterations of endothelial and glial cells in the blood-brain barrier of dystrophic mdx mice. Glia 42:235-251.

Nico B, Paola Nicchia G, Frigeri A, Corsi P, Mangieri D, Ribatti D, Svelto M, Roncali L (2004). Altered blood-brain barrier development in dystrophic MDX mice. Neuroscience 125:921-935.

Nielsen S, Nagelhus EA, Amiry-Moghaddam M, Bourque C, Agre P, Ottersen OP (1997). Specialized membrane domains for water transport in glial cells: high-resolution immunogold cytochemistry of aquaporin-4 in rat brain. J Neurosci 17:171-180.

Noda M (2007). Hydromineral neuroendocrinology: mechanism of sensing sodium levels in the mammalian brain. Exp Physiol 92:513-522.

Noda M, Sakuta H (2013). Central regulation of body-fluid homeostasis. Trends Neurosci 36:661-673.

Okere CO, Waterhouse BD (2004). Capsaicin increases GFAP and glutamine synthetase immunoreactivity in rat arcuate nucleus and median eminence. Neuroreport 15:255-258.

Paxinos G, Watson C (1988).The Rat Brain in Stereotaxic Coordinates, 4th edition, Orlando: Academic Press.

Pixley SK, de Vellis J (1984). Transition between immature radial glia and mature astrocytes studied with a monoclonal antibody to vimentin. Brain Res 317:201-209.

Pócsai K, Bagyura Z, Kálmán M (2010). Components of the basal lamina and dystrophin-dystroglycan complex in the neurointermediate lobe of rat pituitary gland: different localizations of beta-dystroglycan, dystrobrevins, alpha1-syntrophin, and aquaporin-4. J Histochem Cytochem 58:463-479.

Pócsai K, Kálmán M (2014). Extracellular matrix components mark the territories of circumventricular organs. Neurosci Lett 566:36-41

Sanin V, Heeß C, Kretzschmar HA, Schüller U (2013). Recruitment of neural precursor cells from circumventricular organs of patients with cerebral ischaemia. Neuropathol Appl Neurobiol 39:510-518.

Schnitzer J, Franke WW, Schachner M (1981). Immunocytochemical demonstration of vimentin in astrocytes and ependymal cells of developing and adult mouse nervous system. J Cell Biol 90:435-447.

Sisó S, Jeffrey M, González L (2010). Sensory circumventricular organs in health and disease. Acta Neuropathol 120:689-705.

Sixt M, Engelhardt B, Pausch F, Hallmann R, Wendler O, Sorokin LM (2001). Endothelial cell laminin isoforms, laminins 8 and 10, play decisive roles in T cell recruitment across the blood-brain barrier in experimental autoimmune encephalomyelitis. J Cell Biol 153:933-946.

Spoerri O (1963). Concerning the vascularization of the subfornical organ of the rat. Acta Anat (Basel) 54:333-348.

Szabó A, Kálmán M (2004). Disappearance of the post-lesional laminin immunopositivity of brain vessels is parallel with the formation of gliovascular junctions and common basal lamina. A double-labelling immunohistochemical study. Neuropathol Appl Neurobiol 30:169-177.

Szabó A, Kálmán M (2008). Post traumatic lesion absence of beta-dystroglycan-immunopositivity in brain vessels coincides with the glial reaction and the immunoreactivity of vascular laminin. Curr Neurovasc Res 5:206-213.

Tian M, Jacobson C, Gee SH, Campbell KP, Carbonetto S, Jucker M (1996). Dystroglycan in the cerebellum is a laminin α2-chain binding protein at the glial-vascular interface and is expressed in Purkinje cells. Eur J Neurosci 8: 2739-2747.

Uchino M, Hara A, Mizuno Y, Fujiki M, Nakamura T, Tokunaga M, Hirano T, Yamashita T, Uyama E, Ando Y, Mita S, Ando M (1996). Distribution of dystrophin and dystrophin-associated protein 43DAG (beta-dystroglycan) in the central nervous system of normal controls and patients with Duchenne muscular dystrophy. Intern Med 35: 189-194.

Venero JL, Vizuete ML, Machado A, Cano J (2001). Aquaporins in the central nervous system. Prog Neurobiol 63:321-336.

Vígh B, Manzano e Silva MJ, Frank CL, David C, Czirok SJ, Vincze C, Racz G, Lukats A, Szel A (2004). The circumventricular organs of the brain: do they represent a cerebrospinal fluid-dependent regulatory system? Med Hypotheses Res 1:77-100.

Wei LC, Shi M, Chen LW, Cao R, Zhang P, Chan YS (2002). Nestin-containing cells express glial fibrillary acidic protein in the proliferative regions of central nervous system of postnatal developing and adult mice. Brain Res Dev Brain Res 139:9-17.

Wells T (1998). Vesicular osmometers, vasopression secretion and aquaporin-4: a new mechanism for osmoreception? Mol Cell Endocrinol 136:103-107.

Wolburg H, Noell S, Mack A, Wolburg-Buchholz K, Fallier-Becker P (2009). Brain endothelial cells and the glio-vascular complex. Cell Tissue Res 335:75-96.

Yoneda K, Yamamoto N, Asai K, Sobue K, Fujita Y, Fujita M, Mase M, Yamada K, Nakanishi M, Tada T, Miura Y, Kato T (2001). Regulation of aquaporin-4 expression in astrocytes. Brain Res Mol Brain Res 89:94-102.

Zaccaria ML, Perrone-Capano C, Melucci-Vigo G, Gaeta L, Petrucci TC, Paggi P (2001) Differential regulation of transcripts for dystrophin isoforms, dystroglycan, and alpha3A-ChR subunit in mouse sympathetic ganglia following postganglionic nerve crush. Neurobiol Dis 8:513-524.

Zerlin M, Levison SW, Goldman JE (1995). Early patterns of migration, morphogenesis, and intermediate filament expression of subventricular zone cells in the postnatal rat forebrain. J Neurosci 15:7238-7249.